

Efficiently Exploring Adsorption Space to Identify Privileged Adsorbents for Chemical Separations of a Diverse Set of Molecules

Dai Tang,^[a] Ying Wu,^[a, b] Ross J. Verploegh,^[a] and David S. Sholl^{*[a]}

Although computational models have been used to predict adsorption of molecules in large libraries of porous adsorbents, previous work of this kind has focused on a small number of molecules as potential adsorbates. In this study, molecular simulations were used to consider the adsorption of a diverse range of molecules in a large collection of metal–organic framework (MOF) materials. Specifically, 11 304 isotherms were obtained from molecular simulations of 24 different adsorbates in 471 MOFs. This information provides insight into several interesting questions that could not be addressed with previous-

ly available data. Highly computationally efficient methods are introduced that can predict isotherms for a wide range of adsorbing molecules with far less computation than traditional molecular simulations. By characterizing the 276 binary mixtures defined by the molecules considered, “privileged” adsorbents are shown to exist, which are effective for separating many different molecular mixtures. Finally, correlations that were developed previously to predict molecular solubility in polymers are found to be surprisingly effective in predicting the average properties of molecules adsorbing in MOFs.

Introduction

The enormous energy use associated with chemical separations in industrial processes provides a strong incentive to seek more energy-efficient separation methods.^[1] Adsorption-based separations are one broad class of methods that has potential in a wide variety of chemical separations. Although thorough process design is required to fully assess the viability of any putative adsorption process, the ability to consider these processes at even a conceptual level is often limited by the lack of physical properties information. A useful area that has developed rapidly in recent years is the application of computational modeling to predict adsorption in large collections of porous materials. To this end, collections of structures with thousands of experimentally reported zeolites, metal–organic frameworks (MOFs) and related nanoporous materials have been developed.^[2] These collections have been further broadened by far larger sets of hypothetical materials that have been generated *in silico*.^[3]

Numerous examples have been reported that consider gas adsorption in one or more of the materials libraries described

above.^[4] Examples include systematic efforts to characterize adsorption of CO₂,^[4a, 5] CH₄,^[6] noble gases,^[7] and H₂.^[8] Although these studies have considered large numbers of adsorbents, the diversity of the adsorbing molecules that has been considered is low. This situation also applies to extant experimental data. A recent meta-analysis of adsorption isotherms from the open literature showed that the number of adsorbates for which replicate experiments have been reported is low.^[9]

In contrast to the small number of chemical species that have been considered as adsorbates in the studies listed above, the number and diversity of molecular species that exist is enormous. For more than 20 years, methods have existed for generating libraries of more than 100 000 organic compounds for pharmaceutical applications.^[10] Crude oil is known to contain tens of thousands of distinct molecules.^[11] Estimates have been made that there are 10²⁰–10²⁴ different molecules with up to 30 atoms,^[12] and libraries containing over 10¹¹ molecular structures have been developed.^[13] These numbers highlight the observation that developing a fully general understanding of adsorption-based separations will require describing large numbers of possible adsorbent materials and the adsorption of large and diverse collections of molecules in these materials. This challenge can be thought of as the need to explore what might be termed adsorption space.

Herein, we present an initial foray into exploring adsorption space. Specifically, we use molecular simulation methods to predict the room-temperature single-component adsorption isotherms of 24 chemical species with molecular weights up to 140 g mol⁻¹ in a set of 471 MOFs. The resulting set of 11 304 isotherms is similar in size to the collection of experimental isotherms in the NIST/ARPA-E Adsorption Database,^[14] which aims to catalog all isotherms reported in the open literature

[a] Dr. D. Tang, Dr. Y. Wu, Dr. R. J. Verploegh, Dr. D. S. Sholl

School of Chemical & Biomolecular Engineering

Georgia Institute of Technology

311 First Drive NW, Atlanta, Georgia 30332-0100 (USA)

E-mail: david.sholl@chbe.gatech.edu

[b] Dr. Y. Wu

School of Chemical and Chemical Engineering

South China University of Technology

Guangzhou (China)

 Supporting Information (including additional information on the textural properties of the MOFs included in our calculations and data for all of the adsorbate–adsorbent pairs considered herein) and the ORCID identification number(s) for the author(s) of this article can be found under <https://doi.org/10.1002/cssc.201702289>.

and currently contains roughly 14 000 experimental isotherms. Our dataset allows us to examine several interesting questions that could not previously be considered. First, we look at whether it is possible to predict these isotherms with at least moderate accuracy by using minimal computational resources. Our results point towards methods that could readily be applied to predict hundreds of thousands or millions of distinct isotherms. Second, by studying the 276 binary separations that can be defined with the 24 chemical species in our dataset, we ask whether “privileged” adsorbents exist that are effective at separating many different chemical mixtures. Finally, we consider whether correlations that have been developed to describe the solubility of molecules in polymers can also be used to characterize adsorption in crystalline nanoporous materials such as MOFs.

Simulation Details

We used grand-canonical Monte Carlo (GCMC) simulations to calculate single-component adsorption isotherms for a range of molecules in 471 MOFs at 300 K. The MOFs were a subset of the CoRE MOF database,^[2b] which includes considerable diversity in terms of metal nodes, topology, and pore diameters. The 471 structures used in our calculations were the materials fully optimized by Nazarian et al. by using DFT calculations.^[15] Partial charges of framework atoms were assigned by using the DDEC method.^[16] Previous work on these materials has shown that optimization with DFT gives reliable MOF structures and predictions of adsorption isotherms.^[15a,c] Adsorption of each of the 22 organic molecules and 2 noble gases listed in Table 1 was considered in each MOF at 300 K. Most of these species are liquids in the bulk phase at room temperature and pressure. The bulk liquid phase densities at 300 K given in Table 1 were obtained from the TraPPE-UA force field or from the NIST Web Book,^[17] except for species that are supercritical under these conditions, for which the critical density is listed. All GCMC simulations were performed by using RASPA.^[18] Each isotherm was computed up to a pressure ten times larger than the adsorbate’s vapor pressure to ensure that saturation loading in the adsorbed phase was reached. The computational efficiency of GCMC simulations was improved by using the continuous fractional component Monte Carlo method.^[19] 10^5 Monte Carlo cycles were used for the equilibration and production period, respectively, and each cycle included translation, rotation, and reinsertion with equal probability. Preliminary testing indicated that this approach was sufficient to give well-converged results. To give one representative example, our GCMC simulations of octanal in the MOF with structure code FUNCAT included 1.2×10^7 individual MC events with an acceptance probability of about 8% for insertion and deletion moves.

In our GCMC simulations, force-field parameters for the framework atoms were taken from the Universal Force Field (UFF).^[20] This approach has been used in multiple high-throughput computational studies.^[2b,4b,d,5b,6c,21] Force-field parameters for all adsorbates except for Xe and Kr, which were described by UFF^[20] were taken from TraPPE United Atom

Table 1. Molecular weight (MW) and bulk liquid density of each molecule considered for adsorption. Sources for liquid phase densities (LPDs) are noted.

Chemical formula	Name	MW [g mol ⁻¹]	LPD [g cm ⁻³]
CH ₄ ^[26]	methane	16.04	0.16 ^[a]
C ₂ H ₄ ^[17]	ethene	28.05	0.22 ^[b]
C ₂ H ₆ ^[22c, d, 26]	ethane	30.07	0.30 ^[a]
C ₂ H ₃ N ^[22a]	acetonitrile	41.05	0.78 ^[c]
C ₃ H ₈ ^[17, 22g]	propene	42.08	0.50 ^[d]
C ₃ H ₆ O ^[22b]	acetaldehyde	44.05	0.78 ^[c]
C ₃ H ₈ ^[26]	propane	44.10	0.49 ^[e]
C ₂ H ₆ O ^[22b]	dimethyl ether	46.07	0.65 ^[f]
CH ₄ S ^[22e]	methanethiol	48.11	0.86 ^[g]
C ₃ H ₅ N ^[22a]	propionitrile	55.08	0.77 ^[c]
C ₃ H ₆ O ^[22b-d]	acetone	58.08	0.79 ^[c]
C ₃ H ₈ O ^[22f]	propan-1-ol	60.10	0.80 ^[c]
C ₃ H ₈ O ^[22f]	propan-2-ol	60.10	0.79 ^[c]
C ₂ H ₆ S ^[22e]	dimethyl sulfide	62.13	0.85 ^[c]
C ₂ H ₆ S ^[22e]	ethanethiol	62.13	0.86 ^[c]
Kr ^[17, 27]	krypton	83.80	0.91 ^[a]
C ₄ H ₄ S ^[22e]	thiophene	84.14	1.05 ^[c]
C ₅ H ₁₀ O ^[22b]	2-pentanone	86.13	0.81 ^[c]
C ₄ H ₁₀ S ^[22e]	diethyl sulfide	90.19	0.83 ^[c]
C ₇ H ₈ ^[22g]	toluene	92.14	0.87 ^[c]
C ₆ H ₁₄ O ^[22b]	dipropyl ether	102.17	0.75 ^[c]
C ₈ H ₁₆ O ^[22b]	octanal	128.21	0.82 ^[c]
C ₈ H ₁₈ O ^[22f]	octan-1-ol	130.23	0.82 ^[h]
Xe ^[17, 28]	xenon	131.29	1.10 ^[a]

[a] Critical density. [b] Density at 300 K and 4.35 MPa. [c] Density at STP. [d] Density at 300 K and 1.2118 MPa. [e] Density at 300 K and 0.99 MPa. [f] Density at 303 K and 839 kPa. [g] Density at 300 K and 2.20 bar. [h] Density at 300 K and 0.000 018 MPa.

(TraPPE-UA) force field,^[22] which accurately predicts the bulk phase properties for a wide range of molecules. Nonbonding interactions were modeled with cut and shifted Lennard-Jones pair potentials truncated at 12 Å. Except for thiophene (C₄H₄S) and toluene (C₇H₈), two rigid cyclic molecules, all other molecules were described with flexible models including intramolecular interactions for bonds, angles, and torsions. Adsorbate-framework interaction parameters were obtained by using the Lorentz–Berthelot mixing rules. The Ewald summation method was used to calculate electrostatic interactions with a relative precision of 10^{-6} . Each MOF was assumed to be rigid in all calculations. Because we have deliberately focused this study on a broad range of adsorbates, there is essentially no experimental data to which we can directly compare our simulated results. As noted above, the modeling methods we have used have also been the basis of multiple recent high-throughput studies. We also note that the specific choices of generic potentials, mixing rules, and so on were recently shown to make predictions in good consistency with a comprehensive collection of experimentally reproduced adsorption measurements for CO₂ adsorption in MOFs.^[9] This recent work also points to the risks associated with comparing simulated isotherms with experimental measurements that have not been reproduced. The generic potentials we used in our simulations are likely to have limited accuracy in materials that have open metal sites (OMS).^[23] Only 15 of the 471 MOFs we considered have OMS.

These materials are listed in Table S1 (see the Supporting Information). All of the isotherm data from our calculations is available as part of the Supporting Information.

The Henry's law constant for each adsorbate-MOF pair was calculated by using the Widom insertion method.^[24] This calculation requires less computation than performing a GCMC calculation at a single state point.

Some nanoporous crystals can have internal pores that are kinetically inaccessible to adsorption, even though GCMC simulations sample adsorption in these pores. When specific information about which pores are inaccessible is available, GCMC calculations can be made more realistic by blocking these pores. In our view, accurately identifying pores of this kind in a screening study is challenging because examples are well known in which molecules that are considerably larger than the nominal pore size of MOFs in their rigid crystal structures can adsorb.^[25] We therefore did not block any pores in any of the MOFs we simulated.

Results and Discussion

A method for rapid prediction of adsorption isotherms

Although GCMC calculations can be used to predict the details of adsorption isotherms in nanoporous materials like MOFs, it would be useful if the key characteristics of these isotherms could be determined much more rapidly. One of the key aims of our work was to determine whether this goal can be achieved. To this end, we explored the accuracy of an approach that predicts each adsorption isotherm with orders of magnitude less computation than a standard GCMC calculation. Specifically, we modeled each adsorbate-MOF pair as following a Langmuir isotherm [Eq. (1)]:^[29]

$$q(P) = \frac{KP}{1 + \frac{KP}{q_{\text{sat}}}} \quad (1)$$

where K and q_{sat} are the Henry's constant and the saturation loading of the molecule in the MOF.

The Henry's constants at 300 K in the 11 304 adsorbate-MOF pairs we considered are summarized in Figure 1. A number of examples have Henry's constants that are extremely small, typically associated with pores small enough that molecules cannot adsorb without overlapping framework atoms. There are also examples of materials that adsorb selected molecules extremely strongly. The wide range of Henry's constants observed in our calculations illustrates the diversity of the MOFs we examined and provides a useful basis for studying models of adsorption that are valid for a broad range of separations.

The heat of adsorption at infinite dilution, Q , can be computed at the same time the Henry's constant is determined by the Widom insertion.^[30] The heats of adsorption for the examples we considered are summarized in Figure 2. A molecule-MOF pair having a negative heat of adsorption indicates that it is unfavorable for adsorption. This was the case for 6.29% of the examples (711 molecule-MOF pairs) we examined. These

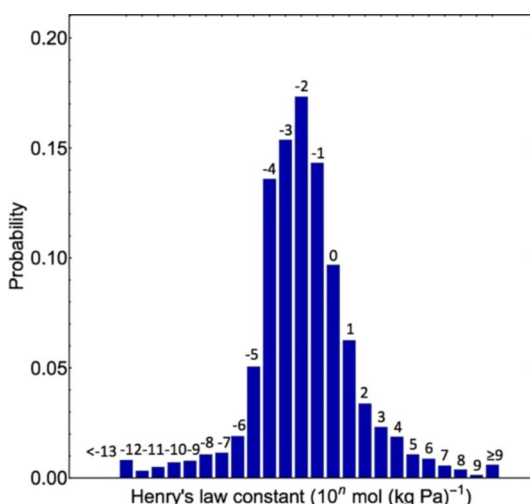


Figure 1. Distribution of Henry's law constants for 24 molecules in 471 MOFs at 300 K. A bar labeled n indicates the examples with Henry's constants in the range 10^{n-1} to $10^n \text{ mol kg}^{-1} \text{ Pa}^{-1}$. The first (last) column includes all examples with Henry's constants smaller than (larger or equal to) 10^{-13} (10^9) $\text{mol kg}^{-1} \text{ Pa}^{-1}$. Approximately 17.33% of the cases we considered have a Henry's constant between 10^{-3} and $10^{-2} \text{ mol kg}^{-1} \text{ Pa}^{-1}$.

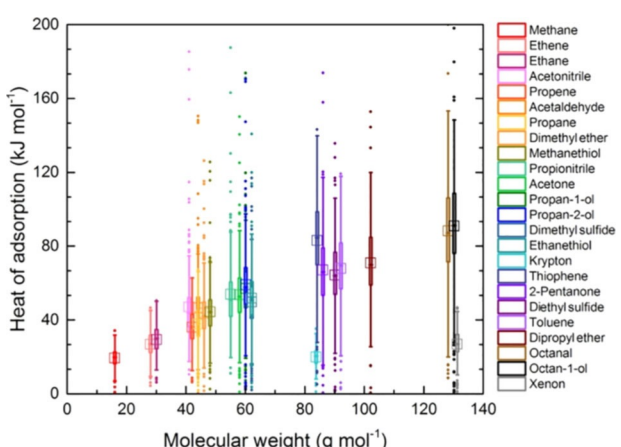


Figure 2. Box and whisker diagrams for the heat of adsorption of each molecule in 471 MOFs. The center line of each box represents the median of data and the square symbol is centered on the mean of data. The upper and lower horizontal lines provide the minimum value ($Q_1 - 1.5 \times IQR$) and maximum value ($Q_3 + 1.5 \times IQR$) respectively, where IQR equals $Q_3 - Q_1$. Outliers beyond this range are shown as individual data points. The data for propan-1-ol and propan-2-ol and for dimethyl sulfide and ethanethiol overlap because the two species have the same molecular weight. Molecule-MOF pairs having negative heat of adsorption are not shown.

cases were excluded from the analysis shown in Figure 2. The resulting heats of adsorption are shown in Figure 2 as a function of the molecular weight (MW) of the adsorbates. As would be expected, there is a generally increasing trend in the heat of adsorption as the MW of the adsorbate increases. The median heat of adsorption increases from $20-30 \text{ kJ mol}^{-1}$ for organic molecules with $MW \approx 16 \text{ g mol}^{-1}$ to more than 80 kJ mol^{-1} for $MW > 120 \text{ g mol}^{-1}$. One notable deviation from the simple trend observed with MW is for thiophene, a cyclic

molecule with a significantly different shape than the other molecules in our test set. We return to this point below. The heats of adsorption for Xe and Kr are significantly less than for molecular species of similar MW. Although MW can be used to rationalize the overall trend in the heats of adsorption, Figure 2 shows that a wide range in this quantity is observed for any given molecule in the full set of MOFs. It is worth noting that once the Henry's constant at 300 K and the heat of adsorption at infinite dilution have been calculated, it is straightforward to predict the Henry's constants at other similar temperatures by using the Van't Hoff equation. This may be a useful alternative to directly simulating the Henry's constant at other temperatures, particularly if information about the Henry's constant as a continuous function of temperature is desired.

To significantly reduce the computational effort associated with calculating the whole isotherm, we initially estimated the saturation loading in each molecule-MOF pair by combining the MOF's void fraction with the molecule's bulk-phase liquid density. The void fraction is commonly calculated by using Widom particle insertion corresponding to the Rosenbluth weight, and using a probe corresponding to helium.^[18b] By using this approach, the adsorption isotherm within the Langmuir approximation can be predicted for all pressures with data from a single low-cost molecular simulation giving the Henry's constant. However, estimating void volume by using a helium atom is potentially imprecise if the size of target adsorbate is quite different. This observation suggests that it is useful to introduce a molecular-size-dependent void fraction into the estimation of the saturation loading. A recent study reported an algorithm of using an adjustable probe size to detect the internal void volume.^[31] Therefore, we characterized the internal void of each MOF by computing what Ongari et al. termed the probe-accessible and probe-occupiable pore volume by using the Zeo++ code version 0.3.^[31–32] The total accessible void fraction is the sum of these two quantities. We calculated the accessible void fraction by varying the probe radius r from 0.01 Å to 2 Å with an interval of 0.02 Å with 10⁵ Monte Carlo moves for each probe size. Crucially, this calculation only has to be performed once for each adsorbent material. An example of the contributions to different volumes shown in Figure S1 indicates that the accessible void fraction decreases approximately linearly with increasing probe radius and eventually jumps to zero when the probe radius is large enough. We then determined the probe-size-dependent scaling factors for the predicted saturation loadings for each adsorbate by fitting our GCMC-simulated results using $Q_{\text{pre,sat}}(r) = k(r)\rho_{\text{liq}}f(r)$. Examples with zero accessible void fraction or negative heat of adsorption were excluded from this fitting procedure. To determine an appropriate probe diameter for each adsorbate, we calculated the mean absolute deviation (MAD) between the actual saturation loading and the scaled estimate of the saturation loading for a set of MOFs and took the optimal probe radius r_{opt} to be the radius that minimized the MAD (Figure S2). The resulting predictions for the saturation loading of diethyl sulfide and xenon in MOFs are shown in Figure 3 as examples. As should be expected, using an adsor-

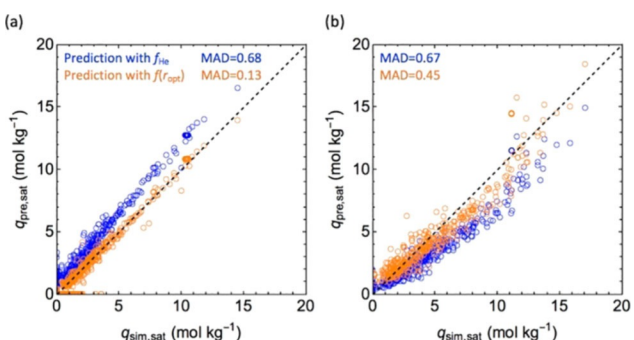


Figure 3. Comparison of simulated saturation loading ($q_{\text{sim,sat}}$) and predicted saturation loading ($q_{\text{pre,sat}}$) for (a) diethyl sulfide ($\text{C}_4\text{H}_{10}\text{S}$) and (b) xenon in 471 MOFs. The blue dots represent the comparison for $q_{\text{pre,sat}} = \rho_{\text{liq}}f_{\text{He}}$ and the orange dots represent the comparison for $q_{\text{pre,sat}}(r_{\text{opt}}) = \rho_{\text{liq}}f(r_{\text{opt}})k(r_{\text{opt}})$. The scaling factor $k(r_{\text{opt}})$ is the slope from a linear fit of $q_{\text{sim,sat}} = k(r_{\text{opt}})q_{\text{pre,sat}}(r_{\text{opt}})$. The accessible void fraction $f(r_{\text{opt}})$ of MOFs and scaling factor $k(r_{\text{opt}})$ used a probe radius of $r_{\text{opt}} = 1.49$ Å for diethyl sulfide and $r_{\text{opt}} = 0.61$ Å for xenon, respectively. The mean absolute deviation (MAD) between the prediction and the adsorption isotherms from GCMC data for a set of MOFs is shown.

bate-dependent probe size significantly improves the quality of the overall fit in each case.

We repeated the scaling analysis and determined the optimal probe radius for each of the 24 molecules. The resulting scaling factors and optimal probe radius are given in Figure 4 and Table S2. We found that the scaling factors decrease as the size of the adsorbate molecules deviates from helium, in part because the larger molecules tend to deviate more strongly from the spherical shape assumed by a probe radius description. This trend is seen in the roughly linear dependence of

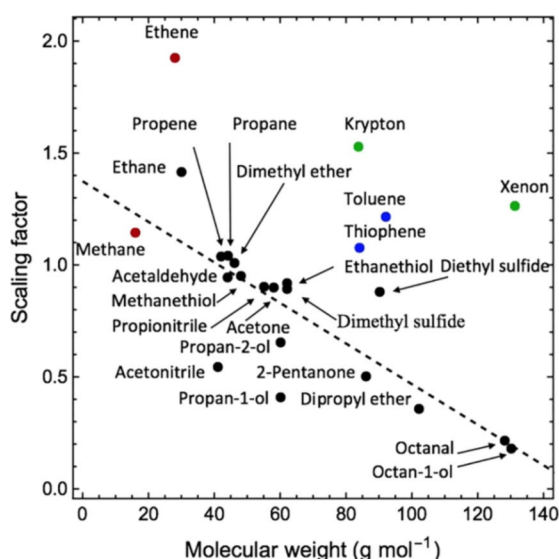


Figure 4. Scaling factor as function of molecular weight. The scaling factor was obtained by using the optimal probe radius of each 24 molecules. The linear fit, which was determined from the condensable species that form bulk liquids at 300 K, shows that the scaling factor tends to decrease with the molecular weight. The non-condensable species (methane and ethene), noble gas molecules (xenon and krypton), and cyclic molecules (thiophene and toluene) are not included in this fit.

the scaling factor on molecular weight. Exceptions from this trend include the two cyclic species we included, thiophene and toluene, since their packing behavior inside the pore differs in a number of ways from linear molecules,^[33] two noble gases, and non-condensable species. It is not surprising that the scaling associated with these classes of molecules is different. An important observation from our calculations is that they were based on a chemically and structurally diverse set of adsorbent materials. As such, we expect that the scaling factors established here would be useful in rapidly estimating the saturation loading of molecules in a very broad range of porous materials without the need to further refine the scaling factors when this approach is applied to larger libraries of materials.

The approach described above provides a method that predicts the isotherm of an adsorbing species at all pressures with high computational efficiency by computing just the Henry's constant of the molecule-MOF pair of interest. It is vital to consider how accurate these predictions are. To quantify the similarity between our predicted and simulated isotherms, we defined the relative error for an isotherm as σ [Eq. (2)]:

$$\sigma = \frac{1}{n} \sum_{i=1}^n \frac{|q_{\text{pre}}(P_i) - q_{\text{sim}}(P_i)|}{q_{\text{sim}}(P_i)} \quad (2)$$

where $q_{\text{pre}}(P_i)$ and $q_{\text{sim}}(P_i)$ are the predicted loading and the simulated loading at pressure P_i , P_i is equal to $10^{-2} P_{\text{vap}}$, $10^{-1} P_{\text{vap}}$, $10^0 P_{\text{vap}}$, and $10 P_{\text{vap}}$ and P_{vap} is the vapor pressure. Figure 5 shows a cumulative plot of the average relative error based on the comparison of each adsorption isotherm from its predicted result and simulated result, which gives the probability level associated with observing the relative error less than a specific value. In the predictions based on the helium void fraction f_{He} for the saturation loadings, 50% of the examples we considered have a relative error of less than 0.29 (median), and the

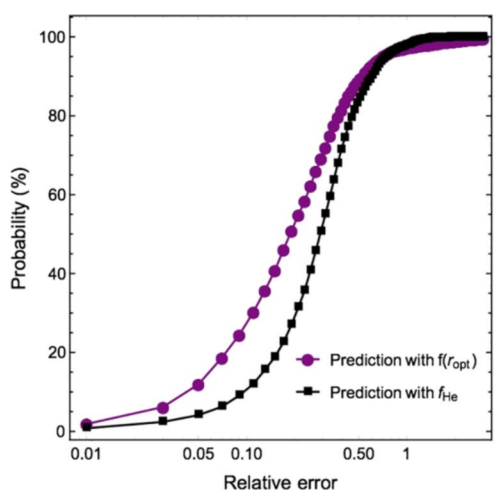


Figure 5. Cumulative plot of relative error of adsorption isotherms for all comparisons of adsorption isotherm between predictions and simulations. The prediction (black) with f_{He} includes all the data except for the cases having negative heat of adsorption and the prediction (purple) with $f(r_{\text{opt}})$ excludes the outliers for each molecule.

range of relative error is between 0.19 (lower quartile) and 0.41 (upper quartile), giving an interquartile range (IQR) of 0.22. By introducing a probe-dependent void fraction and probe-dependent scaling factors into our model, the median, lower quartile, and upper quartile decrease to 0.19, 0.09, and 0.33 respectively. In other words, our methods allow the complete isotherms of 75% of the examples we considered to be predicted within a precision of 33%.

The value of being able to rapidly predict isotherms within a precision of 33% (or any other tolerance) is context dependent. A comprehensive analysis of reproducibility in isotherm measurements for CO_2 adsorption in MOFs recently showed that experimental uncertainties of 10–30% are common for even the most carefully studied materials to date.^[9] Given the time, expense, and uncertainty in measuring the adsorption of complex molecules in MOFs and similar materials, we feel that our results provide an efficient means of rapidly estimating adsorption isotherms at a useful level of precision. It clearly would be interesting to develop methods that improve upon the accuracy shown in Figure 5, and we hope that our data will spur work of this kind. It would be interesting, for example, to examine methods that allow for isotherms other than the Langmuir isotherm that is assumed in our current approach, since adsorbate–adsorbate interactions between many of the molecules we examined seem likely to be of potential importance.

Identification of privileged MOFs for molecular separations

Previous efforts to identify promising MOFs for chemical separations by using large libraries of materials have focused almost exclusively on specific pairs of molecules of practical interest, such as CO_2/N_2 ,^[4a] xylene mixtures,^[34] olefin/paraffin mixtures,^[23d] Xe/Kr ,^[7b] and hexane/heptane.^[35] A question that cannot be answered by studies of this kind is whether MOFs (or other nanoporous materials) exist that are "privileged" for molecular separations. This description borrows a concept from catalysis, where a ligand or catalyst that is effective for a broad range of reactions is described as a privileged catalyst.^[36] For simplicity, we focus on the adsorption of binary mixtures in the dilute limit. At this limit, the selectivity of adsorption is, without approximation, simply the ratio of the Henry's constants of the two adsorbing species.^[37] The adsorption selectivity of a mixture can of course vary as a function of adsorbate loading, but in many situations that selectivity under a wide range of adsorption conditions is accurately characterized by the result from the dilute limit.^[38] The set of 24 molecules that we considered defines 276 unique molecular pairs and we calculated the selectivity at room temperature for each pair in each of the 471 MOFs we considered. Values of selectivity that are much larger or much smaller than 1 indicate adsorbate-MOF combinations with high selectivity.

To assess whether privileged materials for separations exist, we ranked the MOFs for each A–B mixture in descending order by selectivity. To identify the top performers from each list, we gather the top $N_{\text{MOF},\text{pick}}/2$ and the bottom $N_{\text{MOF},\text{pick}}/2$ MOFs in the sorted list for every molecular pair. This procedure gives

the MOFs with the highest selectivity of A over B and the highest selectivity for B over A. We then determined how often each MOF appeared among these lists. The results from this analysis are summarized in Figure 6. The distribution of selectivities that is predicted by our calculations for the 276 molecular pairs we considered is shown in Figure 7a.

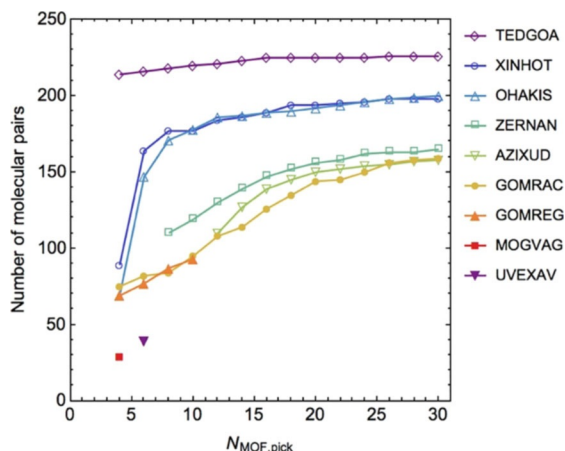


Figure 6. MOFs observed most frequently on ranked lists of MOFs for adsorptive separations of 276 unique molecular pairs as a function of $N_{\text{MOF},\text{pick}}$ (the number of materials selected as “high performers” for each molecular pair).

The results in Figure 6 are remarkable. If the probability of appearing on the “top performer” lists was distributed randomly among the MOFs we examined, a typical MOF would be listed for 6.96 molecular pairs when $N_{\text{MOF},\text{pick}}=10$. In contrast, there are three MOFs shown in Figure 6 that are listed for more than 190 pairs each. The results shown in Figure 6 are insensitive to the specific value of $N_{\text{MOF},\text{pick}}$ used. It is reasonable

to describe each of the materials shown on Figure 6 as “privileged adsorbents.”

The most privileged adsorbent shown in Figure 6 has the structure code TEDGOA. The structure of this material ($[\text{Zn}(\text{HBTT})]\cdot 2 \text{DMA}$, where DMA is *N,N*-dimethylacetamide and HBTT is 1,3,5-tris(2*H*-tetrazol-5-yl)benzene after substitution of two H atoms by DMA), which was named IFMC-6 after its initial synthesis,^[39] is shown in Figure S3. It has rhombus-like 1D channels that are approximately 1 nm^2 in cross-section oriented along the *c* axis. IFMC-6 was synthesized with a view to accommodating Alq₃ chromophores for modulated luminescence but, to our knowledge, it has never been studied for molecular separation.^[40] The identification of this material as an interesting candidate for chemical separations is an example of the value of screening calculations of the kind we have described herein. The selectivity of this material for the 276 molecular pairs we considered is shown in Figure 7b. For comparison, a similar plot for a representative “unprivileged” MOF is shown in Figure 7b. Other privileged materials shown in Figure 6 include the materials with structure codes XINHOT,^[41] OHAKIS,^[42] ZERNAN,^[43] AZIXUD^[44] and GOMRAC.^[45]

Having demonstrated the existence of privileged materials for adsorption, it is reasonable to wonder what the origin of this behavior is in specific materials. Several of the materials listed above have approximately symmetric 1D pores, but there are also examples among our calculations of materials with similar pores that are not among the most privileged materials. For example, FUNCAT,^[46] a pillared paddlewheel MOF material (Figure S4), also has 1D channels with dimensions of roughly 1 nm^2 . When $N_{\text{MOF},\text{pick}}=10$, however, this MOF, which has Zn as metal nodes and 1,2,4,5-tetrakis(4-carboxyphenyl)-benzene (H4TCPB) and 3,6-bis(methoxycarbonyl)-1,2,4,5-tetrazine as linkers, does not appear on the ranked lists for any molecular pairs in our calculations. In their seminal description of privileged catalysts, Yoon and Jacobsen noted that “it is not

immediately clear what structural features account for the broad applicability of privileged structures across so many different reaction types”.^[36] It seems likely that this description will also apply to privileged adsorbents for separations.

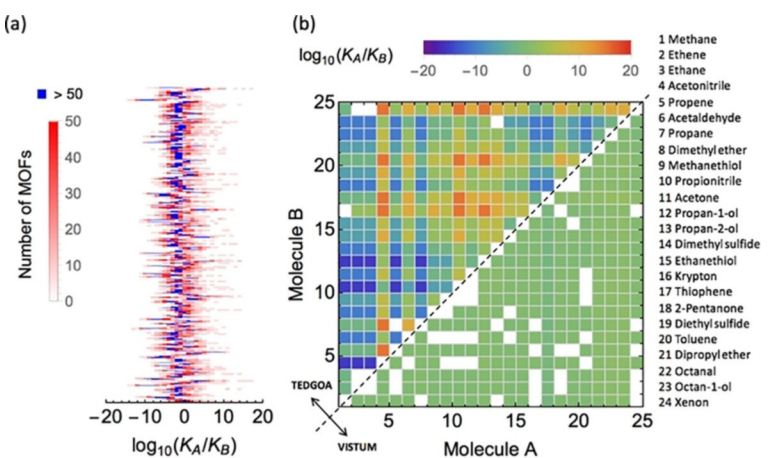


Figure 7. a) Vertical stacking of distributions of MOF's selectivities on 276 distinct molecular pairs, demonstrating the range of predicted selectivities that are observed. b) The privileged MOF TEDGOA (upper left triangle) shows stronger adsorptive separation than one of average-performing MOFs VISTUM (lower right triangle) for most molecular pairs. Pairs with identical molecules or negative heat of adsorption in both molecules are marked in white.

Simple correlations for adsorption selectivity in MOFs

The above discussion of privileged materials focused on finding the best-performing materials for adsorption-based chemical separations. It is also interesting to consider whether simple descriptions exist can be developed to characterize the typical selectivity that can be expected in MOFs. Descriptions of this kind are known for molecular solubility in polymers, a topic that has been widely studied. For polymers, the relative solubility of pairs of condensable species in a polymer and the difference of their Lennard-Jones temperatures can be fitted by using Equation (3).^[47]

$$\ln\left(\frac{S_i}{S_j}\right) = N\left(\epsilon_i/k - \epsilon_j/k\right) \quad (3)$$

The prefactor, N , in this expression is found to be independent of the polymer and takes a universal value of 0.023 K^{-1} . To test the relevance of this simple model for molecular adsorption in MOFs, we replaced the solubility and Lennard-Jones temperature in Equation (3) by the Henry's constant from our computed isotherms and the molecule's critical temperature, to give Equation (4):

$$\ln\left(\frac{K_i}{K_j}\right) = N(T_{c,i} - T_{c,j}) + C \quad (4)$$

A constant was included in the model in addition to the term proportional to the difference in critical temperatures. The data fitted by this model is summarized in Figure 8a, where a fit to Equation (3) gives $N=0.0245\text{ K}^{-1}$ and a fit to Equation (4) gives $N=0.0245\text{ K}^{-1}$ and $C=0.0648$. The small value of C indicates that the functional form of Equation (3) is adequate to fit the data. A surprising feature of this analysis is that the scaling constants for polymers and for MOFs are very similar. That is, in the absence of any other information, the adsorption selectivity for a molecular pair in a typical MOF is quite similar to the adsorption selectivity of the same pair in a typical polymer. This observation potentially masks some details that are likely to be important. First, our results for molecular pairs involving thiophene or toluene differ markedly from the data for all other molecular pairs (Figure 8a). This indicates that a simplistic description, such as Equation (3) or (4), is not likely to be adequate for all possible molecular pairs. Also, the variation of observed selectivities around the average values predicted from Equation (3) or (4) is large, with many examples that differ from the average values by multiple orders of magnitude. This situation is illustrated by Figure 8b, where the distribution of selectivities among the MOFs we considered is shown for three representative molecular pairs. In many instances,

it will be materials that lie towards the extremes of these distributions that are the most interesting, since they correspond to the most selective materials for a given molecular separation.

Conclusions

This study represents an initial step towards the challenge of fully exploring adsorption space by using molecular simulations of a diverse set of 24 molecules adsorbing in 471 MOFs. These simulations extend previous computational studies of adsorption, which have focused on one or at most a few adsorbing species. For each of the 11304 adsorbate–adsorbent pairs that we considered, a full room-temperature adsorption isotherm was predicted by using GCMC simulations. We also examined the adsorption selectivity for the 259992 possible binary mixture–adsorbent pairs defined by our data at the limit of low loadings.

One use of our large dataset is to explore computationally efficient methods to predict adsorption isotherms in even larger collections of adsorbates or adsorbents. We showed that an approach that uses only the Henry's constant for an adsorbate–adsorbent pair, the liquid phase density of the adsorbate in the bulk phase and some textural information about the adsorbent can predict most isotherms with similar accuracy to what is available in typical experiments. This approach, or future refinements of these ideas, could potentially be used to predict isotherms for millions of adsorbate–adsorbent pairs, a task that is critical to fully explore adsorption space that is unlikely to be achieved by brute-force computation.

We also examined some implications of our dataset for separations of chemical mixtures. By using an analogy from previous work on catalysis, we introduced the concept of a privileged adsorbent, which is a material that is highly effective for a large number of different chemical separations. Because of the sparse nature of the available data, it has not previously been possible to assess whether or not privileged adsorbents exist. Our analysis strongly suggests that materials of this kind do exist. As is the case for the many years of work that has been devoted to privileged catalysts, it is not clear what underlying physical mechanisms or characteristics distinguish these materials from other less highly performing materials. Nonetheless, the fact that these materials exist at all is extremely interesting. It is important to note that our ranking of the “best” materials was based on a single metric, namely the adsorption selectivity. Development of materials for practical applications must of course also consider a host of other factors, such as regenerability, adsorption capacity, and stability in process conditions.^[15a,48]

A final use we made of our dataset was to compare the adsorption properties of molecules in MOFs with gas solubilities in polymers. A surprising observation is that the average adsorption properties of the molecules we examined in MOFs can be described with very similar correlations to those that have been reported previously for solubility in polymers. It is important to note, however, that the variation around the average among the set of MOFs we considered is very large,

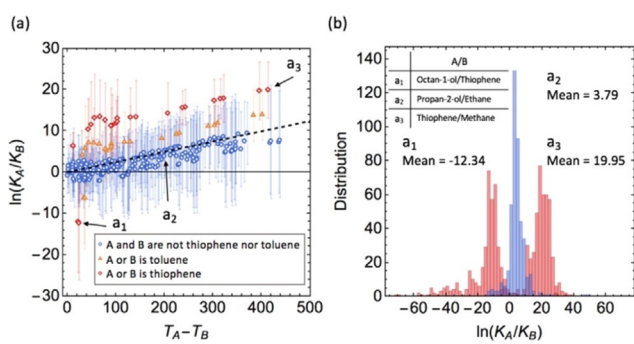


Figure 8. a) The median and standard deviation (error bars) of the log of Henry's constant ratio for each molecular pair (error bars) as a function of the critical temperature difference. Freeman's model is used to fit all data, giving the fitted $N=0.0245\text{ K}^{-1}$ (dashed black line) with the mean of absolute standardized residuals $R^2=2.35$. Pairs including toluene (orange triangle) or thiophene (red diamond) deviate far from the majority of data (blue dots). b) Number distribution of MOFs for $\ln(K_A/K_B)$.

so the average properties provide only the most qualitative of information.

Several caveats must be considered to put our results in a broader perspective. Our simulations rely on generic force fields because of the chemical diversity of the materials we examined. A considerable body of work exists on developing quantitatively accurate force fields for molecular adsorption in nanoporous materials,^[23d,49] but these methods are not yet transferrable between diverse classes of materials. Our models necessarily describe defect-free materials, although real materials inevitably include defects of various kinds that may in some cases influence adsorption, especially at dilute loadings.^[50] Our simulations only described single-component adsorption, whereas for separations applications it is always multicomponent adsorption that is of interest. We discussed binary selectivities at the limit of dilute loadings and, at this limit, the selectivities obtained from our calculations are exact.^[37] At higher loadings, mixing theories, such as Ideal Adsorbed Solution Theory, can be used to predict multicomponent adsorption from single component data,^[37] but the accuracy of this approach for highly non-ideal mixtures is unclear. GCMC simulations are well suited to detailed treatment of multicomponent adsorption once specific examples of interest are identified, but it will be challenging to systematically use this approach for the diverse sets of molecules we have started to explore in this study. Finally, there are several issues beyond simply equilibrium isotherms that dictate whether a separation process is practically and economically viable, for example the long term stability of the adsorbent in the presence of possible trace contaminants and the cost and availability of the adsorbent at scale.^[48] Despite all of these caveats, we feel that the breadth of data available from our results opens up long-term possibilities that will be useful in connecting the concept of exploring adsorption space with the development of practical adsorption-based separation processes.

Acknowledgements

D.T. and D.S.S. were supported by the Department of Energy Nanoporous Materials Genome Center, supported by the U.S. Department of Energy, Office of Basic Energy Sciences, Division of Chemical Sciences, Geosciences and Biosciences under Award DEFG02-12ER16362 and used resources of the Argonne Leadership Computing Facility, which is a DOE Office of Science User Facility supported under Contract DE-AC02-06CH11357. R.J.V. received support from the National Science Foundation grant number 1604375. Y.W. thanks the China Scholarship Council (CSC) (No. 201506150058) for a fellowship to visit the Georgia Institute of Technology.

Conflict of interest

The authors declare no conflict of interest.

Keywords: adsorption • high-throughput screening • metal-organic frameworks • molecular modeling • separations

- [1] a) D. S. Sholl, R. P. Lively, *Nature* **2016**, *532*, 435–437; b) R. P. Lively, D. S. Sholl, *Nat. Mater.* **2017**, *16*, 276–279.
- [2] a) K. S. Park, Z. Ni, A. P. Côté, J. Y. Choi, R. Huang, F. J. Uribe-Romo, H. K. Chae, M. O’Keeffe, O. M. Yaghi, *Proc. Natl. Acad. Sci. USA* **2006**, *103*, 10186–10191; b) Y. G. Chung, J. Camp, M. Haranczyk, B. J. Sikora, W. Bury, V. Krungleviciute, T. Yildirim, O. K. Farha, D. S. Sholl, R. Q. Snurr, *Chem. Mater.* **2014**, *26*, 6185–6192; c) R. Pophale, P. A. Cheeseman, M. W. Deem, *Phys. Chem. Chem. Phys.* **2011**, *13*, 12407–12412.
- [3] a) D. A. Gomez-Gualdrón, O. V. Gutov, V. Krungleviciute, B. Borah, J. E. Mondloch, J. T. Hupp, T. Yildirim, O. K. Farha, R. Q. Snurr, *Chem. Mater.* **2014**, *26*, 5632–5639; b) Y. Bao, R. L. Martin, M. Haranczyk, M. W. Deem, *Phys. Chem. Chem. Phys.* **2015**, *17*, 11962–11973.
- [4] a) E. Haldoupis, S. Nair, D. S. Sholl, *J. Am. Chem. Soc.* **2012**, *134*, 4313–4323; b) T. Watanabe, D. S. Sholl, *Langmuir* **2012**, *28*, 14114–14128; c) E. Haldoupis, S. Nair, D. S. Sholl, *Phys. Chem. Chem. Phys.* **2011**, *13*, 5053–5060; d) Y. J. Colón, R. Q. Snurr, *Chem. Soc. Rev.* **2014**, *43*, 5735–5749.
- [5] a) J. Park, R. P. Lively, D. S. Sholl, *J. Mater. Chem. A* **2017**, *5*, 12258–12265; b) Z. Qiao, K. Zhang, J. Jiang, *J. Mater. Chem. A* **2016**, *4*, 2105–2114.
- [6] a) C. E. Wilmer, M. Leaf, C. Y. Lee, O. K. Farha, B. G. Hauser, J. T. Hupp, R. Q. Snurr, *Nat. Chem.* **2012**, *4*, 83–89; b) Y. He, W. Zhou, G. Qian, B. Chen, *Chem. Soc. Rev.* **2014**, *43*, 5657–5678; c) D. A. Gómez-Gualdrón, C. E. Wilmer, O. K. Farha, J. T. Hupp, R. Q. Snurr, *J. Phys. Chem. C* **2014**, *118*, 6941–6951; d) C. M. Simon, J. Kim, D. A. Gomez-Gualdrón, J. S. Camp, Y. G. Chung, R. L. Martin, R. Mercado, M. W. Deem, D. Gunter, M. Haranczyk, D. S. Sholl, R. Q. Snurr, B. Smit, *Energy Environ. Sci.* **2015**, *8*, 1190–1199.
- [7] a) T. Van Heest, S. L. Teich-McGoldrick, J. A. Greathouse, M. D. Allendorf, D. S. Sholl, *J. Phys. Chem. C* **2012**, *116*, 13183–13195; b) D. Banerjee, C. M. Simon, A. M. Plonka, R. K. Motkuri, J. Liu, X. Chen, B. Smit, J. B. Parise, M. Haranczyk, P. K. Thallapally, *Nat. Commun.* **2016**, *7*, 11831; c) C. M. Simon, R. Mercado, S. K. Schnell, B. Smit, M. Haranczyk, *Chem. Mater.* **2015**, *27*, 4459–4475; d) B. J. Sikora, C. E. Wilmer, M. L. Greenfield, R. Q. Snurr, *Chem. Sci.* **2012**, *3*, 2217–2223.
- [8] M. P. Suh, H. J. Park, T. K. Prasad, D. W. Lim, *Chem. Rev.* **2012**, *112*, 782–835.
- [9] J. Park, J. D. Howe, D. S. Sholl, *Chem. Mater.* **2017**, *29*, 10487–10495.
- [10] L. A. Thompson, J. A. Ellman, *Chem. Rev.* **1996**, *96*, 555–600.
- [11] A. G. Marshall, R. P. Rodgers, *Acc. Chem. Res.* **2004**, *37*, 53–59.
- [12] P. Kirkpatrick, C. Ellis, *Nature* **2004**, *432*, 823.
- [13] R. Visini, M. Awale, J. L. Reymond, *J. Chem. Inf. Model.* **2017**, *57*, 700–709.
- [14] *NIST/ARPA-E Database of Novel and Emerging Adsorbent Materials, NIST Standard Reference Database 205* (Eds.: D. W. Siderius, V. K. Shen, R. D. Johnson, III, R. D. van Zee), National Institute of Standards and Technology, Gaithersburg, MD, 2015; <https://adsorption.nist.gov/srd205/index.php> (accessed March 13, 2018).
- [15] a) D. Nazarian, J. S. Camp, D. S. Sholl, *Chem. Mater.* **2016**, *28*, 785–793; b) D. Nazarian, P. Ganesh, D. S. Sholl, *J. Mater. Chem. A* **2015**, *3*, 22432–22440; c) D. Nazarian, J. S. Camp, Y. G. Chung, R. Q. Snurr, D. S. Sholl, *Chem. Mater.* **2017**, *29*, 2521–2528.
- [16] a) T. A. Manz, D. S. Sholl, *J. Chem. Theory Comput.* **2011**, *7*, 4146–4164; b) T. A. Manz, D. S. Sholl, *J. Chem. Theory Comput.* **2012**, *8*, 2844–2867.
- [17] P. J. Linstrom, W. G. Mallard, *The NIST Chemistry WebBook*, National Institute of Standards and Technology, Gaithersburg, MD; <http://webbook.nist.gov> (accessed March 13, 2018).
- [18] a) A. Torres-Knoop, S. P. Balaji, T. J. H. Vlugt, D. Dubbeldam, *J. Chem. Theory Comput.* **2014**, *10*, 942–952; b) D. Dubbeldam, S. Calero, D. E. Ellis, R. Q. Snurr, *Mol. Simul.* **2016**, *42*, 81–101.
- [19] W. Shi, E. J. Maginn, *J. Chem. Theory Comput.* **2007**, *3*, 1451–1463.
- [20] a) M. A. Addicoat, N. Vankova, I. F. Akter, T. Heine, *J. Chem. Theory Comput.* **2014**, *10*, 880–891; b) A. K. Rappe, C. J. Casewit, K. S. Colwell, W. A. Goddard, W. M. Skiff, *J. Am. Chem. Soc.* **1992**, *114*, 10024–10035.
- [21] S. Li, Y. G. Chung, R. Q. Snurr, *Langmuir* **2016**, *32*, 10368–10376.
- [22] a) C. D. Wick, J. M. Stubbs, N. Rai, J. I. Siepmann, *J. Phys. Chem. B* **2005**, *109*, 18974–18982; b) J. M. Stubbs, J. J. Potoff, J. I. Siepmann, *J. Phys.*

- Chem. B* **2004**, *108*, 17596–17605; c) M. Dinpajoooh, P. Bai, D. A. Allan, J. I. Siepmann, *J. Chem. Phys.* **2015**, *143*, 114113; d) A. D. Cortés Morales, I. G. Economou, C. J. Peters, J. I. Siepmann, *Mol. Simul.* **2013**, *39*, 1135–1142; e) N. Lubna, G. Kamath, J. J. Potoff, N. Raj, J. I. Siepmann, *J. Phys. Chem. B* **2005**, *109*, 24100–24107; f) B. Chen, J. J. Potoff, J. I. Siepmann, *J. Phys. Chem. B* **2001**, *105*, 3093–3104; g) C. D. Wick, M. G. Martin, J. I. Siepmann, *J. Phys. Chem. B* **2000**, *104*, 8008–8016.
- [23] a) N. Lamia, M. Jorge, M. A. Granato, F. A. Almeida Paz, H. Chevreau, A. E. Rodrigues, *Chem. Eng. Sci.* **2009**, *64*, 3246–3259; b) Y. S. Bae, C. Y. Lee, K. C. Kim, O. K. Farha, P. Nickias, J. T. Hupp, S. T. Nguyen, R. Q. Snurr, *Angew. Chem. Int. Ed.* **2012**, *51*, 1857–1860; *Angew. Chem.* **2012**, *124*, 1893–1896; c) A. L. Dzubak, L. C. Lin, J. Kim, J. A. Swisher, R. Poloni, S. N. Maximoff, B. Smit, L. Gagliardi, *Nat. Chem.* **2012**, *4*, 810–816; d) A. R. Kulkarni, D. S. Sholl, *J. Phys. Chem. C* **2016**, *120*, 23044–23054.
- [24] B. Widom, *J. Chem. Phys.* **1963**, *39*, 2808–2812.
- [25] R. J. Verploegh, S. Nair, D. S. Sholl, *J. Am. Chem. Soc.* **2015**, *137*, 15760–15771.
- [26] M. G. Martin, J. I. Siepmann, *J. Phys. Chem. B* **1998**, *102*, 2569–2577.
- [27] F. Theeuwes, R. J. Bearman, *J. Chem. Thermodyn.* **1970**, *2*, 179–185.
- [28] F. Theeuwes, R. J. Bearman, *J. Chem. Thermodyn.* **1970**, *2*, 507–512.
- [29] L. C. Lin, A. H. Berger, R. L. Martin, J. Kim, J. A. Swisher, K. Jariwala, C. H. Rycroft, A. S. Bhown, M. W. Deem, M. Haranczyk, B. Smit, *Nat. Mater.* **2012**, *11*, 633–641.
- [30] a) F. Karavias, A. L. Myers, *Langmuir* **1991**, *7*, 3118–3126; b) T. J. H. Vlugt, E. Garcia-Perez, D. Dubbeldam, S. Ban, S. Calero, *J. Chem. Theory Comput.* **2008**, *4*, 1107–1118.
- [31] D. Ongari, P. G. Boyd, S. Barthel, M. Witman, M. Haranczyk, B. Smit, *Langmuir* **2017**, *33*, 14529–14538.
- [32] T. F. Willems, C. H. Rycroft, M. Kazi, J. C. Meza, M. Haranczyk, *Microporous Mesoporous Mater.* **2012**, *149*, 134–141.
- [33] a) R. Krishna, *Phys. Chem. Chem. Phys.* **2015**, *17*, 39–59; b) A. Torres-Knoop, J. Heinen, R. Krishna, D. Dubbeldam, *Langmuir* **2015**, *31*, 3771–3778.
- [34] J. A. Gee, K. Zhang, S. Bhattacharyya, J. Bentley, M. Rungta, J. S. Abichandani, D. S. Sholl, S. Nair, *J. Phys. Chem. C* **2016**, *120*, 12075–12082.
- [35] Y. G. Chung, P. Bai, M. Haranczyk, K. T. Leperi, P. Li, H. Zhang, T. C. Wang, T. Duerinck, F. You, J. T. Hupp, O. K. Farha, J. I. Siepmann, R. Q. Snurr, *Chem. Mater.* **2017**, *29*, 6315–6328.
- [36] T. P. Yoon, E. N. Jacobsen, *Science* **2003**, *299*, 1691–1693.
- [37] K. S. Walton, D. S. Sholl, *AIChE J.* **2015**, *61*, 2757–2762.
- [38] S. R. Challa, D. S. Sholl, J. K. Johnson, *J. Chem. Phys.* **2002**, *116*, 814–824.
- [39] G. S. Yang, M. N. Li, S. L. Li, Y. Q. Lan, W. W. He, X. L. Wang, J. S. Qin, Z. M. Su, *J. Mater. Chem.* **2012**, *22*, 17947–17953.
- [40] a) C. Y. Sun, X. L. Wang, C. Qin, J. L. Jin, Z. M. Su, P. Huang, K. Z. Shao, *Chem. Eur. J.* **2013**, *19*, 3639–3645; b) R.-B. Lin, H.-L. Zhou, C.-T. He, J.-P. Zhang, X.-M. Chen, *Inorg. Chem. Front.* **2015**, *2*, 1085–1090; c) W. Xie, W. W. He, D. Y. Du, S. L. Li, J. S. Qin, Z. M. Su, C. Y. Sun, Y. Q. Lan, *Chem. Commun.* **2016**, *52*, 3288–3291.
- [41] D.-C. Hou, G.-Y. Jiang, Z. Zhao, J. Zhang, *Inorg. Chem. Commun.* **2013**, *29*, 148–150.
- [42] A. Aijaz, E. Barea, P. K. Bharadwaj, *Cryst. Growth Des.* **2009**, *9*, 4480–4486.
- [43] J. Z. Gu, J. Wu, D. Y. Lv, Y. Tang, K. Zhu, J. Wu, *Dalton Trans.* **2013**, *42*, 4822–4830.
- [44] C. Q. Li, W. G. Qiu, H. He, *Acta Crystallogr. Sect. E* **2011**, *67*, m1406.
- [45] X. Song, Y. Li, L. Gan, Z. Wang, J. Yu, R. Xu, *Angew. Chem. Int. Ed.* **2009**, *48*, 314–317; *Angew. Chem.* **2009**, *121*, 320–323.
- [46] O. K. Farha, C. D. Malliakas, M. G. Kanatzidis, J. T. Hupp, *J. Am. Chem. Soc.* **2010**, *132*, 950–952.
- [47] B. D. Freeman, *Macromolecules* **1999**, *32*, 375–380.
- [48] K. S. Walton, D. S. Sholl, *Joule* **2017**, *1*, 208–211.
- [49] a) A. R. Kulkarni, D. S. Sholl, *Langmuir* **2015**, *31*, 8453–8468; b) K. D. Vogiatis, E. Haldoupis, D. J. Xiao, J. R. Long, J. I. Siepmann, L. Gagliardi, *J. Phys. Chem. C* **2016**, *120*, 18707–18712; c) V. Bernales, A. B. League, Z. Li, N. M. Schweitzer, A. W. Peters, R. K. Carlson, J. T. Hupp, C. J. Cramer, O. K. Farha, L. Gagliardi, *J. Phys. Chem. C* **2016**, *120*, 23576–23583; d) D. R. Pahls, M. A. Ortuno, P. H. Winegar, C. J. Cramer, L. Gagliardi, *Inorg. Chem.* **2017**, *56*, 8739–8743; e) J. G. McDaniel, S. Li, E. Tylianakis, R. Q. Snurr, J. R. Schmidt, *J. Phys. Chem. C* **2015**, *119*, 3143–3152; f) J. G. McDaniel, J. R. Schmidt, *Annu. Rev. Phys. Chem.* **2016**, *67*, 467–488.
- [50] D. S. Sholl, R. P. Lively, *J. Phys. Chem. Lett.* **2015**, *6*, 3437–3444.

Manuscript received: December 4, 2017

Revised manuscript received: March 13, 2018

Version of record online: April 17, 2018